Neuroscience Informatics 2 (2022) 100019

Contents lists available at ScienceDirect

Neuroscience Informatics

www.elsevier.com/locate/neuri

NaaS

Classification of optimal brain tissue using dynamic region growing and fuzzy min-max neural network in brain magnetic resonance images

Sunil L. Bangare

Department of Information Technology, Sinhgad Academy of Engineering, Savitribai Phule Pune University, Pune, India

ARTICLE INFO

Article history:
Received 1 October 2021
Received in revised form 12 October 2021
Accepted 20 October 2021

Keywords:
Fuzzy min max neural network
Gabor filtering
Segmentation
Modified region growing
Optimization
Fruit-fly
Region merging

ABSTRACT

On an MRI scan of the brain, the boundary between endocrine tissues is highly convoluted and irregular. Outdated segmentation algorithms face a severe test. Machine learning as a new sort of learning Here, researchers categorize normal and abnormal tissue using the fuzzy min-max neural network approach, which helps classify normal and abnormal tissues such as GM, CSF, WM, OCS, and OSS. This classification helps to explain the fuzzy min-max neural network method. Osseous Spongy Substance, SCALP, and Osseous Compact Substance are all MRI-classified as aberrant tissue in these tissues. Denoising and improving images can be accomplished using the Gabor filtering technique. Using the filtering method, the tumour component will be accurately identified during the segmentation operation. A dynamically changed region growing approach may be applied to a picture by modifying the Modified Region Growing method's two thresholds. This helps to raise Modified Region Growing's upper and lower bounds. Once the Region Growth is accomplished, the edges may be observed using the Modified Region Growing segmented image's Edge Detection approach. After removing the texture, an entropy-based method may be used to abstract the colour information. After the Dynamic Modified Region Growing phase findings have been merged with those from the texture feature generation phase, a distance comparison within regions is performed to combine comparable areas in the region merging phase. After tissues have been identified, a Fuzzy Min-Max Neural Network may be utilised to categorise them.

1. Introduction

Medical Imaging is a promising tool for exhibiting the internal body in detail. In order to assess and diagnose human health and illness, it is widely used by the radiologist [1,3]. It's possible to determine the activities and functions of the brain using three different imaging modalities: computed tomography (CT), magnetic resonance imaging (MRI), and ultrasound. When it comes to radiology, the MRI scan is noninvasive, radiation free, and more advanced than CT and X-Ray since it can look in several directions and identify multiple dimensions simultaneously. [2,4]. With regard to radiologists' understanding of patient brain behaviour, MRI (Magnetic Resonance Imaging) will play an increasingly important role in the future. It features various compensations, including excellent imaging resolution, sound detection, soft tissue consideration, and identifying scanning variance, among others [4].

Tissue's intricate edifices make image segmentation a critical job. For the purpose of forming and detecting a brain tumour, this is a very compelling objective. There are two types of brain tumours: malignant and benign. Because of its well-defined borders and lack of ingrainedness in brain tissue, a benign tumour may be removed surgically. Brain tumours that are malignant develop and spread far quicker than benign ones, and they can be devastating [5]. As multimodal MRI scans provide a wealth of information about tumours, radiologists are clamouring for them to separate brain tumour images from normal ones. Schizophrenia, MS, Parkinson's disease, and Alzheimer's disease are just a few of the conditions that may be diagnosed using magnetic resonance imaging (MRI) pictures.

MR scans of the brain typically separate the white matter (WM), grey matter (GM), and cerebrospinal fluid (CSF) into three distinct tissue types [6]. In brain diagnostic systems, these three areas are especially useful for detecting diseases, planning treatments, defining anatomy, and computer-aided neurosurgery [7]. Classification methods for tissues may roughly be divided into supervised and unsupervised categories. Semi-automatic refers to a technology that still requires human input to be controlled. It's important to keep in mind that the unsupervised segmentation is completely automated and has a high density of segments in

E-mail address: sunil.bangare@gmail.com.

https://doi.org/10.1016/j.neuri.2021.100019

feature space Brain tumours in the early stages can be seen on MRI scans. It is possible for MRI to create weighted images that are distinct to one another to better depict the unique properties of various tissues. These MRI sequences are commonly used: T1-weighted, T2-weighted, and Flair-weighted. Brain MRI categorization has been the subject of several investigations. Neural networks, fuzzy c-means, genetic algorithms, k-nearest neighbours, and support vector machines (SVM) are some examples of these techniques [9].

Multilayer Perceptron (MLP) is the most often used kind of Neural Network in Artificial Neural Network (ANN) implementations. The architecture of a neural network differs from that of a microprocessor, and the method takes a long time to complete. The popularity of fuzzy c-means can be attributed to its ease of use and simplicity of calculation. Different geometric forms might cause problems for FCM when trying to identify partitioning, such as compact hyper-ellipses, ring-shaped clustered objects, or hyper-ellipsoids with a different geometric shape. FCM's Euclidean distance depreciation helps detect hyper-spherical clusters that are unreliable when dealing with real-world problems. Because it is more noise-resistant than FCM, the Gaussian Kernel distance in FCM has been substituted and extended [10]. A kernel-based supervised classification approach called Support Vector Machines (SVM) has been widely used in the categorization of medical hyperspectral images. To achieve better accuracy than unsupervised, the administered classification technique in SVM relies on labelled data provided by the end user.

2. Literature survey

This study considered a number of recent publications on the use of MRI to classify tissue. Using a hierarchical design of K-Nearest Neighbour classifiers, Piero Baraldi et al. [12] predicted a diagnostic system that could detect deterioration early on and isolate the deteriorating bearing while classifying the fault kind. The Western Reserve Case University Bearing dataset's real-world vibrational information has been put to good use in experiments conducted on deteriorated pathways. For the industrialised approach to be successful, bearing deterioration in automobiles must be reproduced in experiments that mimic real-world driving conditions.

Nonparametric supervised spectral-spatial classification methods for multispectral images have been proposed by Zhlobin Cui et al. [13]. Due to its superior presentation, the developed technique uses Gaussian Mixture Model (GMM) instead of Single Gaussian Model (SGM) for sifting training datasets. Sequences of trials on the innovative Bayesian strategy have been used to handle the projected technique, which shows superior representation than other classification approaches, such as Min-DC, MDC, MLC, MLR, and SVM.

Using an automated process, Alireza Ghaemia et al. [14] have developed an industrialised methodology for reducing complexity in Brain-Computer Interfaces (BCI). They made use of the Improved Binary Gravitation Search Algorithm (IBGSA) to detect the operating electroencephalography (EEG) channels mechanically in the left or right hand categorization. As a consequence of IBGSA, they were able to determine the best route to take in order to get higher categorization results. An average accuracy of 76.24 percent was observed among eight distinct participants. MRI image segmentation and classification research for abnormality recognition is sparse in the literature. Because of its critical implementations, it's become a hot issue. A basic overview of medical picture segmentation and classification algorithms is provided at this time.

There is a technique proposed by Bianchi et al. [16] that integrates high-level contextual information with visual data at low levels in order to perceive mTBI lesions. Using subject data, such as the time since injury and information of the site of mTBI, this contextual model predicts disease development. An MRI texture feature model and a probabilistic support vector machine are used in the visual model, which takes use of the discriminating in unimodal MR images. A final evaluation of the mTBI lesion sites is obtained by bonding these two models together in a 3D environment. A rodent model of recurrent mTBI is used to test the models' predictions. It was discovered from the research results that the merging of contextual and visual textural characteristics outperforms all other approaches currently in use. Clinicians will gain from the speedier diagnosis, and patients will profit from the refinement of clinical treatment thanks to the approach's clinical benefits.

Pre-operative and post-recurrence brain MR images of glioma patients were studied by Kwon et al. [17] and a strategy for deformable registration was proposed. Because tumours, resections, recurrence and swelling create substantial deformations in the images, missing correspondences and irregular intensity profiles, doing this type of intra-subject registration was exhilarating. An innovative approach called PORTR, which expressly takes into consideration abnormal data, was developed to deal with this challenging issue. Tumor, resection cavity, and recurrence are all segmented using models tailored to the specifics of each CAT scan. By quantifying the overlap between an aligned tumour and resection cavity, PORTER may exclude problematic areas from his image-based correspondence term. Using both discrete and continuous search techniques, they pursued the best possible outcome while remaining within the constraints of the registration system.

Specialized medical imaging required unique software and professional skills. These researchers [18] have proposed a cheap general-purpose image processing tool that's easy to use, as well as visualisation software built specifically in MATLAB to catch as many brain diseases as feasible in the early stages. Clinical and quantitative medical picture analysis are both provided by the implementation. Schizophrenia, epilepsy, hereditary speech and language problems, and Alzheimer's dementia are only a few of the serious conditions caused by slight anatomical differences in the brain. The primary objective was to examine the connection between Alzheimer's disease and the brain's psychological character.

Islam et al. [19] developed a stochastic model for classifying tumour texture in brain MR images using random variables. The model's effectiveness was demonstrated in the abstraction of brain tumour textural features and tumour segmentation in magnetic resonance images without the involvement of a patient (MRIs). A multi-resolution fractal model termed multi-fractional Brownian motion was used to create brain tumour texture because of the MRI's complicated appearance (mBm). On the other hand, an abstract spatially-varying multi-fractal feature abstract mathematical derivation for the MB model is planned. Next, a brain tumour segmentation method based on several fractal features was put into production. Efficacy was evaluated by correlating tumour segmentation performance with the use of Gabor like multi-scale texton feature launched with the assistance of launched multi-fractal. In addition, a tumour segmentation system that is independent of the patient was envisioned by using the well-known Ada-Boost algorithm. Classifier weights are assigned to component classifiers according to how well they are able to classify complicated data and how confident they are in doing so. This approach was tested on fourteen individuals and shown to be effective in automatically segmenting tumours in brain MRIs with over three hundred MRIs.

Zacharaki and Bezerianos et al. [20] have established a semi-supervised system for the identification and segmentation of medical picture anomalies. Due to the lack of a pathologic model, semi-administered learning allows for more automation. If a vector

does not follow the probability distribution derived from regular information, it is called abnormal in abnormality identification. However, due to the enormous complexity of the information, estimating the probability density function was seldom possible. The images were stored as a network of adjacent coherent picture partitions to tackle this problem (overlapping blocks). They used a distributed estimation technique to satisfy the consistency criteria while expressing and optimising a highly concave probability function for identifying irregularity in each division. The probability function was a quadratic programming problem comprised of a model and an information term. Automatic segmentation of brain diseases such simulated infarction and dysplasia was achieved using the approach. Fa Zhu et al. [11] shown the use of weights for SVM. Zafer Iscan et al. [15] used segmentation techniques. Christakis Damianou et al. [21] explains the MRI things. Selva Bhuvaneswari et al. [22] proposed the classification with region growing methods. Daniel Schwarz et al. [23] discussed the new method for morphometry. In addition, diabetes patients' real lesions, cloud computing research was presented by [30] [31] M. L. Bangare et al. In light of security issues, LMI Leo Joseph et al. [34] developed deep learning techniques.

High-intensity focused ultrasound (HIFU) in newly excised lamb brain and rabbit brain was studied by Damianou et al. in vivo using magnetic resonance imaging (MRI). A 5 cm diameter single-element spherically absorbed transducer operating at one megahertz was used to focus at a distance of 10 cm The transducer was circumnavigated using a prototype MRI-compatible positioning device. T1-W and T2-W fast spin-echo (FSE) and fluid-attenuated inversion recovery were used to evaluate the effects of HIFU (FLAIR). However, T2-W FSE and FLAIR show more anatomical features in the brain than T1-W FSE, but with T1-W FSE, both thermal and bubbly lesions had a higher contrast between the lesion and the brain. Kamal Gulati and colleagues discussed their IoT and user interface research. [24] [33], respectively. Researchers S. L. Bangare et al. [25] [26] [27] [28] [32] [36] [38], raised the issue of machine learning's scalability problems. Md Khairul Islam et al. [39] claim that a template-based K-means algorithm with superpixels and principle component analysis (PCA) quickly and accurately detects human brain cancer. Rajesaheb R. Kadam et al. [29], Sachindra K. Chavan et al. [30], Manoj L. Bangare et al. [31] [37] and Shashikant Athawale et al. [35] have shown great research approach to solve the realistic issues.

G. Ramkumar et al. [40] present the Deep Convolutional Neural Network Algorithm (DCNNA) to explore all sorts of 3X3 kernel sections. According to similarity co-efficient metrics, the suggested technique to Brain Tumor Segmentation using DCNNA produces good results between 0.886 and 0.777 for similarity co-efficients.

In machine learning and AI, Linjuan Ma et al. [41] To begin, instead of using a traditional neural network, the network makes use of a lightweight neural network to balance accuracy against efficiency. Second, in addition to predictive intelligence, we've included edge intelligence into our plans to make medical data centres' deployment and processing easier.

3. Problem definition

The organization of medical images is a significant stage for most image-related implementation and visualization tasks. It assists medical doctors in detecting the diseases inside the body without the surgery process, decreases the image reading time, sees the location of a lesion, and regulates an estimation of the probability of disease. The standard issue of available image segmentation and tissue classification method is provided below,

- Although there has been a great deal of study, segmentation leftovers remain a difficult problem because of the various picture content, crowded objects, occlusion, image noise, uneven object texture, and other issues. Numerous algorithms and approaches are available for image segmentation, however progress toward a quick and accurate method of brain MRI tissue segmentation is still required.
- An image segmentation method with the help of region growing requires initial seeds selection that upsurges computational cost & execution time.
- The primary issue of the available classification and segmentation technique is the accuracy issue.
- One of the main difficulties appears manual assortment of the seed pixels or regions.

These are the chief disadvantages of various available works as shown in (Fig. 1) that motivate us to research image segmentation and classification. The general architecture for our projected study is mentioned below (Fig. 1),

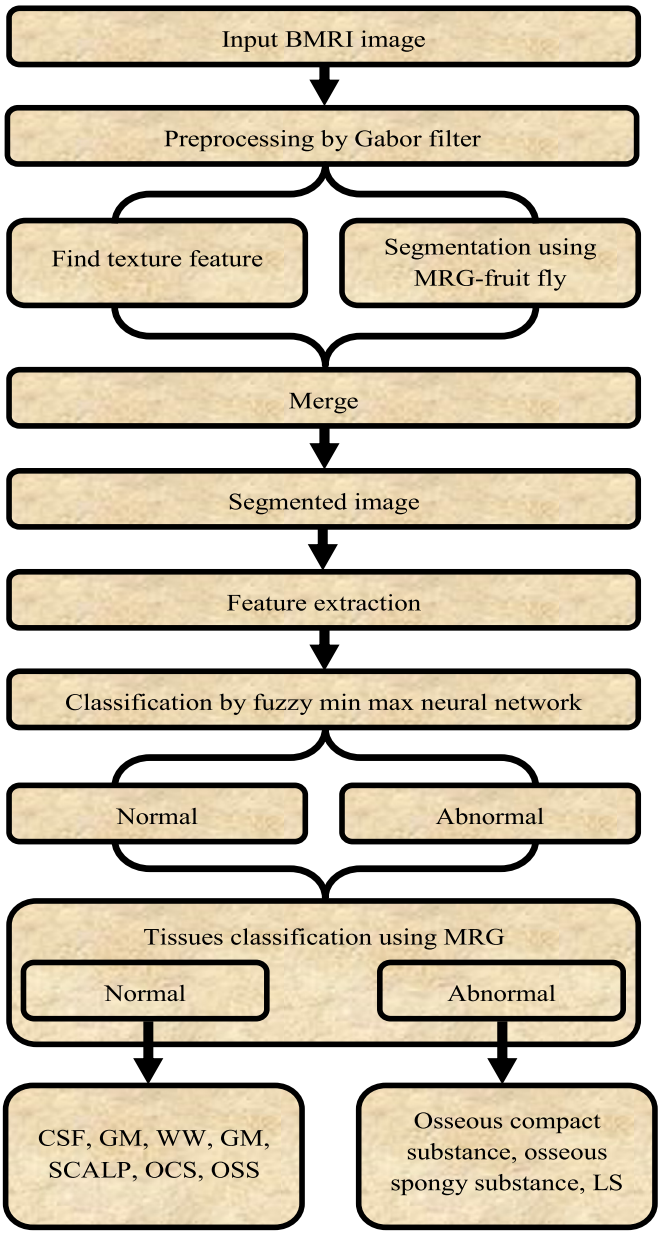

Fig. 1. Proposed optimal tissue classification in brain MRI image.

4. Proposed methodology

Basic principles used in MRI picture categorization include brain MRI tissue segmentation. During the segmentation process, there are four phases: pre-processing; threshold generation with dynamic modified region growing; texture feature generation; and region merging. It is possible to denoise and enhance pictures with Gabor filtering. Using the filtering approach ensures that the tumour is accurately identified throughout the segmentation process. The first phase of the input picture may be achieved as the Dynamic Modified Region Growing technique by dynamically adjusting two thresholds in the Modified Region Growing process. The Fruit Fly method, an optimization technique, helps to improve Modified Region Growing's two thresholds: yield and quality. The Edge Detection technique can detect the edges once the Region Growth segmented picture has been obtained using Modified Region Growing. The texture feature may be extracted from the input picture in the second phase using entropy-based operations. The outputs of the texture feature creation phase and the dynamic modified region growing phase are combined in the region merging phase. When comparing distances within regions, you're comparing regions that are similar. Once the tissues have been identified, a Fuzzy Min-Max Neural Network may be used to classify them. K-cross fold validation technique will be used to analyse the expected approach's performance in detail. Multiple Brian MRI scans will be used to test the suggested method in Matlab.

4.1. Pre-processing

For the most part, pre-processing refers to the operations that must be performed before the primary objective inquiry and abstraction of the unique real image's expected statistical and generally geometric adjustments can be performed. These improvements include of correcting information for errors and removing unwanted ambient noise from non-brain element images, as well as translating information to accurately replicate the original image.

4.1.1. Gabor filter

It is possible to denoise and enhance pictures with Gabor filtering. With the filtering mechanism in place, it will be possible to identify tumour parts with pinpoint accuracy throughout the segmentation process A Gaussian function multiplied by a harmonic function defines the impulse response of Gabor filters, which are linear filters. Numerous image processing techniques, such as face identification, texture segmentation, and iris pattern description, benefit greatly from Gabor filter responses. The uncertainty principle's minimal space-bandwidth product is one of these filters' most important rewards. As a result, they now provide simultaneous optimum resolution in the spatial and spatial frequency domains, as well as both. Problems with segmentation arising from complex pictures with embedded textured regions can be solved with Gabor filters. In terms of feature extraction, Gabor filters have a wide range of useful or even better features. Gabor filters are linear filters with a different name. Convolution in the spatial domain is the simplest way to do the filtering process. A picture was convolved with the Gabor elementary performances to get the unique appearances. The complicated sinusoidal modulated grating of a two-dimensional gabor function.

$$g(x, y) = \frac{1}{2\pi\omega^2} \exp\left\{-\frac{(x^2 + y^2)}{2\omega^2}\right\} \exp\left[j2\pi(u_x + v_y)\right] \quad (1)$$

For $\omega_x = \omega_y, = \omega$ the parameters ω_x and ω_y are the space constants of the Gaussian envelop along x and y axes, correspondingly.

Gabor Filtered image as o_h is provided as,

$$o_h\big(i(x, y)\big) = \big[i(x, y) \otimes h(x, y)\big] \quad (2)$$

This time, the method from the pre-processed picture output is texture feature abstraction and segmentation in these segmentation procedures may be done with Modified Region Growing-Fruitfly algorithm where input image $i(x, y)$ and function $h(x, y)$ are both 2-D Gaussian functions.

4.2. Texture feature generation

The input picture IR generates the texture feature. The textured region has an uncertainty value associated with it, which makes it easier to merge the regions using the same representative across all of them. This preliminary ambiguity is linked to the pixel area. Before any other quantization can take place, however, the input infrared picture must be divided evenly into tiny boxes measuring 9*9. Each block in the picture has its own entropy.

In order to calculate the entropy, divide the number of pixels by the number of pixels in the image, then multiply the two numbers by the number of pixels in the image. $p(A_j)$ represents the probability that a certain value A_j will occur, and it contains $I(A_j)$ data points. As seen in eqn (3), the data unit is clearly specified.

$$I(A_j) = \log \frac{1}{p(A_j)} = -\log p(A_j) \quad (3)$$

Thus, $I(A_j)$ of the whole pixel set in one block of image is found and then the entropy of each block of the image can be intended as in the Equation (4).

$$E(s) = -\sum_{j=1}^{s} p(A_j) \log p(A_j) \quad (4)$$

The resultant value is assigned to the block's centre pixel for use in creating the texture feature after the entropy value is computed for each block in the picture. As a result, the image's texture feature may be obtained, and the image's texture is denoted as IT.

4.3. Threshold generation with modified region growing

The threshold technique is the classification of each pixel depends on its data like intensity and colour data. Those measures are proficient when the histogram of objects and background are separated. In a thresholding-based segmentation system, each image is alienated into several segments by describing some threshold value. The threshold is a very known and straightforward method for segmentation in computer vision and image investigation. At this time, the segmentation procedure will be accomplished with the help of region-based segmentation.

4.3.1. Region based segmentation

Segmentation methods based on region are simpler and more noise-resistant when it comes to edge detection. Edge-based techniques divide an image into areas that are analogous based on a set of predetermined criteria, whereas region-based approaches divide an image due to the fast variations in intensity around the picture's edges. The following approaches are primarily used in region-based segmentation algorithms:

Region growing

One of the most often used segmentation strategies is the region-growing method. This method starts with a seed pixel and grows the region by adding nearby pixels based on a threshold

value to the seed pixel itself. When a region's expansion slows, a new seed pixel is selected and the process is restarted using a pixel that is not part of any other region. It's possible to stop the area from expanding once all of the pixels have been allocated. Small, basic features like tumours and lesions may be clearly delineated using region growing segmentation. Many restrictions apply while utilising this method, including the following: Manual selection of the seed location is required in some cases. In the abstracted regions, noise sensitivity causes gaps or excess segmentation. The area growth method may separate the discontinuity in the abstracted image. During this period, the system establishes an image threshold. The system can obtain two thresholds from this point on. The system can capture a single threshold from these thresholds. The system will next use the region-growing approach to combine these criteria. Region merging will also abstract a texture-based feature, and a fruit-fly method will be used to optimise it.

Region merging

Region merging uses pictures from the Modified region growth and texture feature creation phases. Therefore, the region merger processes are detailed as follows:

- ***Pixel replacing*:** Before doing pixel replacement on the MRG picture's pixels, have a look at the foreground pixels (the image generated in phase I, IMRG). The grey pixels of the IR picture are extracted and then substituted for the MRG image pixels by this IR image grey pixel. In this way, grey pixels replace the MRG picture pixels, resulting in an IP-style image.
- ***Distance calculation*:** In the place of the MRG picture, the distance between each pixel was replaced by IP and texture images in IT. The Euclidean distance metric is utilised for the distance evaluation. By using this metric, every pixel in these two sets of pictures is evaluated as shown in the equation below.

$$\mathrm{I(p,t)} = \sum_{i=1}^{N} Ipi - ITi \tag{5}$$

An image is combined after a threshold value is established for the distance between pixels in pixel replaced MRG image (IP), pixel replaced Ip (IT) and texture image IT (IT). If the distance between pixels is less than the threshold value, pixels are set to 0; otherwise, pixels are set to 1. As a result, the identical pixel areas in the MRG image, IP, and texture image IT are combined using the pixel distance assessment. For the given input image, the first step can be achieved as a Dynamic Modified Region Growing procedure by dynamically altering the two thresholds in the modified region growing method. The optimization algorithm, Fruit Fly algorithm, helps to enhance both of these thresholds within Modified Region Growing.

Fruit-fly optimization algorithm

FFOA, or the Fruit-Fly Optimization Algorithm, is another useful tool for studying fruit fly behaviour. The fruit fly's olfactory and visual senses are superior to those of other species in terms of perception and recognition. Fruit flies' olfactory organs can detect a wide spectrum of odours in the air surrounding them, and they can even detect food sources 40 kilometres distant. Using its sensitive vision, it can find the food and the rushing arena of the organisation after drawing close to it. Then it can fly to that area and eat. The fruit fly's food-finding method may be condensed into the following steps: (1) First, the fruit fly uses its factory organ to detect the food supply and then flies towards that position; (2) Next, it uses its sensitive visions to approach close to the food source; (3) Finally, it uses the fruit fly's flocking location and flies in that direction.

Steps of fruit fly algorithm

Step 1: FFOA starting settings include the total number of evolutions, population size, and the beginning position where fruit flies form swarms. Fruit flies represent the value of a feature in the method we suggest. Initialize random location of a fruit fly (FU_{axis}, FV_{axis}).

Step 2: Exploration with the help of arbitrary path and detachment to the olfactory organ.

$$\mathrm{FU}_m = FU_{axis} + Rand \tag{6}$$

$$\mathrm{FV}_m = FV_{axis} + Rand \tag{7}$$

Step 3: The food's position is unknown; therefore first the distance (D) from the beginning is calculated. Next, the computed value of the scent concentration is computed, which is termed the reverse of distance (S_C).

$$\mathrm{D_m} = \sqrt{\left(FU_m^2 + FV_m^2\right)} \tag{8}$$

$$\mathrm{S}_{C\mathrm{m}} = 1/D_m \tag{9}$$

Step 4: Substitute smell concentration value (S_C) into fitness function just to perceive the smell concentration of every fruit flies position.

$$Fitness = function(S_{Cm}) \tag{10}$$

Step 5: Perceive the location of the most excellent smell concentration (highest value).

$$[\text{Excellent Smell Excellent Index}] = \mathrm{M}ax\left(\text{function}(\mathrm{S_{Cm}})\right) \tag{11}$$

Step 6: Preserves the highest smell concentration value and (*FU*, *FV*) coordinate, then the fruit fly swarm flies towards the location with the maximal smell concentration value. The fruit fly swarm will use visualization to flutter in that direction.

$$\text{Smell Excellent} = \text{Excellent Smell} \tag{12}$$

$$\mathrm{FU\_}axis = FU(Excellent\ index) \tag{13}$$

$$\mathrm{FV\_}axis = FV(Excellent\ index) \tag{14}$$

Step 7: Assume that the scent concentration is greater than previous consecutive smell concentrations by using sequential optimization to replicate their execution in stages 2-5. If this is the case, then use this fruit-fly method to complete job 6. A region merging process joins texture feature generation results with Dynamic Modified Region outcomes obtained before. A distance comparison within regions is used to combine growing phases and related areas. Fuzzy Min-Max Neural Network may be used to classify the tissues once they have been recognised. Finally, the system assimilates the textures' abstracted and segmented images before performing a feature extraction method using GLCM from the resulting merged segmented picture.

4.4. Feature extraction

- **Grey level co-occurrence matrix (GLCM)**

The number of rows and columns in a GLCM correspond to the image's total number of grey levels, G. The matrices element represents the separated pixel distances that correlate (d1 and d2). The GLCMs are capable of obtaining sufficient statistics from them using the grey co-props function, which provides the following details about an image's texture. Energy

a. Entropy
b. Contrast
c. Correlation

Energy: There are squares for each entry in the GLCM. This is called the Angular Second Moment, and it shows the sum of the squares for each entry. The term 'uniformity' is used to describe it. With an energy range of [0.1], we know exactly where we are. A fixed image's energy value is equal to one. The following is the energy assessment equation:

$$Energy = \sum_{x,y} p(x,y)^2 \tag{15}$$

where, $p(x, y)$ is the pixel value at the point x, y of the texture image of size $(M \times N)$

Entropy: When it comes to representing texture images and controlling how the distribution changes in different parts of the image, entropy comes in handy. Image disturbance may be accurately assessed using the consistent parameter. Many GLCM rudiments have low utility when the picture is not textually identical, revealing that the entropy is very high. The following Equation calculates the entropy.

$$Ent = \sum_{x,y} p(x,y)\log\big(p(x,y)\big) \tag{16}$$

Contrast: It's abbreviated as CON. Contrast is also known as 'Sum of Square Variance.' A pixel's intensity contrast with that of its neighbouring pixels is calculated and submitted throughout the entirety of the picture. The picture contrast value is 0 when the image is constant. Weight, on the other hand, increases exponentially (0, 1, 4, 9) as long as one sticks with the diagonal.

$Range = [0, size\ (GLCM, 1) - 1)^2]$.

$$Contrast = \sum_{i,j=0}^{N-1} p_{i,j}(i-j) \wedge 2 \tag{17}$$

Since the contrast increases (i-j), it continues to grow exponentially. The case when I and j have the same value, that is, $i - j = 0$. There isn't even a hint of contrast. When I and j are shifted by a factor of 1, a minor difference appears. When the difference between I and j is 2, the contrast widens and the weight goes up by one.

Correlation: Because it is possible to calculate the correlation between a pixel and its neighbouring pixels over the whole picture, linear dependence between grey levels may be determined. The correlation score is 1 or -1 for an easily positively or negatively linked picture. On behalf of constant image its value is $NaN..Range = [-1, 1]$ and the formula is,

$$Correlation = \sum_{i,j=0}^{N-1} p_{i,j}\left[\frac{(i-\mu i)(j-\mu j)}{\sqrt{(\sigma i^2)(\sigma j \wedge 2)}}\right] \tag{18}$$

4.5. Fuzzy min max neural network

Fuzzy min-max learning can either expand or contract. A collection of ordered pairs (A, I) is used as the training data, with $A = A1, A2...An$ being the input data and $I = 1, 2, ...m$ being the class index. To begin, choose an ordered pair and locate a hyper box for the same class that can expand to incorporate the input if necessary. If the expansion conditions cannot be met by an existing hyper box, a new hyper box is created and added to the network. A hyper box's minimum and maximum points are used to define the membership function. To put it another way, it tells you how well a pattern fits within the hyper box. Each of the hyper boxes has a 0–1 value range. The hyper box has a unity membership function for patterns inside of it. Each hyper box's definition is defined mathematically. The fuzzy set Hj [8] has the following definition:

$$H_j = \left\{A, V_{\min_j}, W_{\max_j}, F(A, V_{\min_j}, W_{\max_j})\right\} \tag{19}$$

where,

A - Input data,

$V_{minj}(V_{min1}, V_{min2}, \ldots V_{minN})$ is the minimum points of H_j
$W_{maxj}(W_{max1}, W_{max2}, l \ldots W_{maxN})$ is the maximum points of H_j
$F(A, V_{mini}, W_{maxi})$ is the membership function

The membership function for the *jth* hyperbox (H_j) is given below,

$$H_j = \frac{1}{2n}\sum_{i=1}^{n}\big[\max\big(0, 1 - \max\big(0, \gamma \min(1, A_i - w_{ij})\big)\big) + \max\big(0, 1 - \max\big(0, \gamma \min(1, v_{ji} - A_i)\big)\big)\big] \tag{20}$$

where, as the distance between A and Hj grows, a sensitivity parameter γ controls how quickly the membership value drops. There are three node layers in a fuzzy min max neural network. The topmost layer represents the data input layer. The last layer denotes the output layer, which contains the total number of classes to be produced.. The hyper box layer refers to the centre or hidden layer of an object. A fuzzy min max neural network may be used to classify the normal from the abnormal in this situation. Afterwards, a tissue classification is carried out with the assistance of MRG, which classifies normal and pathological tissues such as CSF and osseous compact material, osseous spongey substance, as well as scalp, GM, WM, and scale.

5. Result and discussion

To classify Fuzzy min max neural networks, we use the suggested brain MRI tissue categorization. The suggested technique's performance is compared to that of the currently used DWT-GWO methods.

5.1. Experimental results

The suggested picture for tissue classification is based on a variety of real-world and medical imagery. Brain MRI pictures and medical images were utilised as real-world examples. The pictures are sent into the algorithm as input and are separated into categories including CSF, GM, ML, OCS, SCALP, and WM, which are used to classify normal and abnormal images, respectively. Modified Region Growing does the segmentation. A fuzzy min-max neural network may be used for classification, and modified region growth can be used to classify normal and pathological tissues in the end.

Sensitivity: Sensitivity is defined as the percentage of true positives that are correctly identified. It has to do with a test's ability to identify positive findings.

$$\text{Sensitivity} = \frac{\text{TP}}{(\text{TP} + \text{FN})}$$

where TP stands for True Positive and FN stands for False Negative

Table 1
Truth table for experimental outcome.

Experimental outcome	Condition as determined by the standard of Truth	
	Positive	**Negative**
Positive	**TP**	**FP**
Negative	**FN**	**TN**

Table 2
Performance analysis for our proposed technique.

Proposed	'CSF'	'GM'	'ML'	'OCS'	'OSS'	'Scalp'	'WM'
Accuracy	0.96	0.89	0.98	0.94	0.99	0.967	0.93
Sensitivity	0.98	0.99	1	0.99	0.99	0.99	0.96
Specificity	0.23	0.16	0.05	0.08	0	0.07	0.3

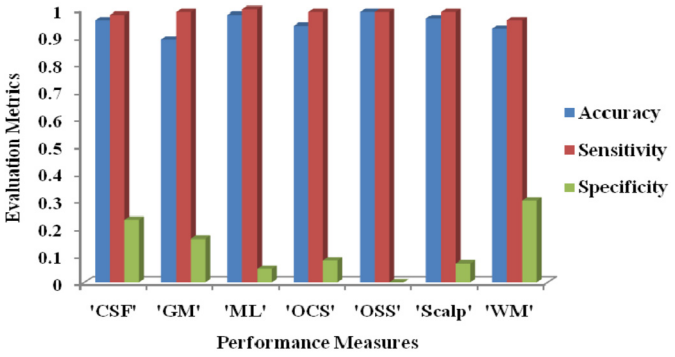

Fig. 2. Graph for performance analysis for our proposed technique.

Specificity: The amount to which negatives are appropriately identified is the measure of specificity. It has to do with a test's ability to detect negative findings.

$$\text{Specificity} = \frac{\text{TN}}{(\text{TN} + \text{FP})}$$

where TN stands for True Negative and FP stands for False Positive.

Accuracy: TP and TN total number to total quantity of data ratio is the accuracy of the suggested technique.

$$\text{Accuracy} = \frac{\text{TN} + \text{TP}}{(\text{TN} + \text{TP} + \text{FN} + \text{FP})}$$

5.2. Performance analysis

The suggested approach's performance will be assessed using Sensitivity, Specificity, and Accuracy once classification is completed using fuzzy min-max neural network technique. There are several performance measures in Table 1 that demonstrate how well we've done in terms of our intended research.

Table 2 and Fig. 2 show that brain MRI image segmentation based on tissue categorization has good segmentation ratio values for the BMRI pictures, which the system can deduce from the data. CSF, GM, ML, OCS, OSS, SCALP, and WM are examples of categorised tissues. All tissues have an accuracy of 0.95 percent, and all tissues have a sensitivity of 0.98 percent, and all tissues have a specificity of 0.127 percent. It is clear that the suggested approach may be used to classify medical and real-world pictures of all tissues.

Accuracy, sensitivity, and specificity may be determined from the above-mentioned tabular value II and Fig. 3 (Table 3). Training and testing values such as 70-30, 80-20, and 90-10 have been used in the suggested approach. For 70-30 training and testing values,

Table 3
Performance measures based on training and testing data.

Training and testing	Accuracy	Sensitivity	Specificity
70-30'	0.956521739	0.888888889	1
'80-20'	0.913043478	0.9	0.923076923
'90-10'	0.909090909	0.87	1

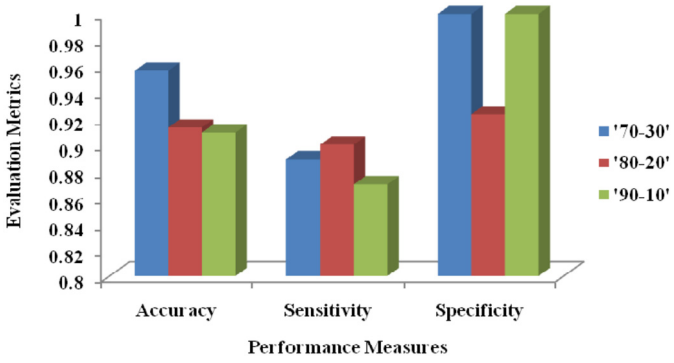

Fig. 3. Graph for performance measures taken based on training and testing.

Table 4
Proposed and existing comparison accuracy obtained based on training and testing values.

Training and testing	Existing MRG	Proposed MRG-FF
'70-30'	0.801304348	0.956521739
'80-20'	0.859090909	0.913043478
'90-10'	0.796363636	0.909090909

Table 5
Proposed and existing sensitivity obtained tissue classification.

Training and testing	Existing MRG	Proposed MRG-FF
'70-30'	0.888888889	0.888888889
'80-20'	0.73	0.9
'90-10'	0.8	0.87

accuracy comes to 0.9565, for 80-20 training and testing values to 0.9130, and for 90-10 training and testing to 0.9090 for specificity to come to 0.9090.

5.3. Comparative analysis along with results and discussion

In order to demonstrate that the suggested MRG-Fruitfly algorithm-based tissue categorization work is superior to the existing MRG technique, the two methods are put side by side. Tables 5 and 6 show the changed region developing as the old one does in this part, which is demonstrated in the previous work.

Fig. 4 compares the categorization results for brain MRI images solely between the proposed and current methods.

Table 4 in Fig. 4 shows that the suggested approach efficiently identified a tissue with superior quality and high accuracy, based on all of the aforementioned assessment findings for accuracy comparison. When our suggested MRG-FF algorithm is put side by side with the currently used MRG methodology, the results will show that our approach is superior.

Table 5 in Fig. 5 shows that the suggested technique accurately identified a tissue with superior quality and high specificity based on the aforementioned assessment findings for accuracy comparison. Compared to the existing MRG methodology, our suggested method will produce superior outcomes when compared to the proposed MRG-FF algorithm.

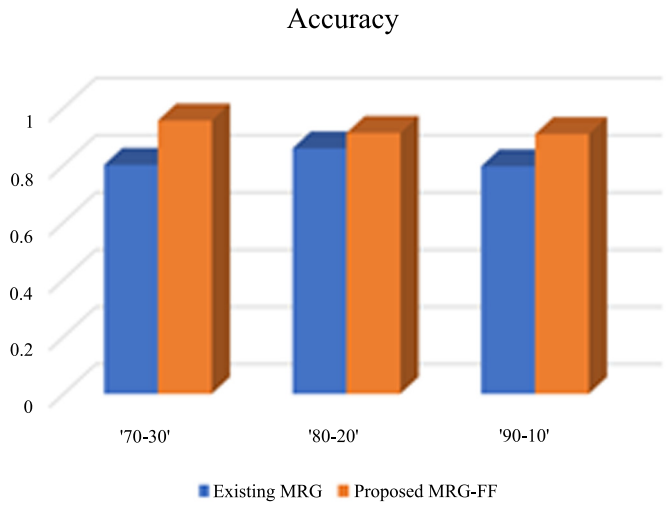

Fig. 4. Graph for proposed and existing accuracy obtained based on training and testing values.

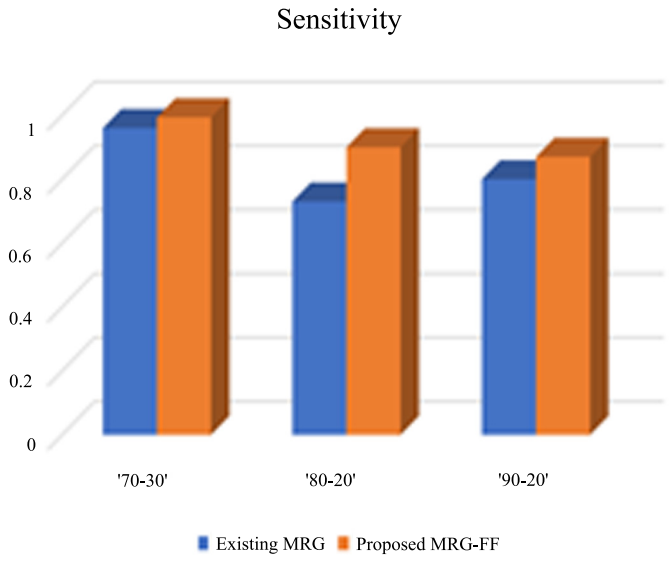

Fig. 5. Graph for proposed and existing sensitivity value taken based on training and testing values.

Table 6
Proposed and existing specificity value taken based on training and testing values.

Training and testing	Existing MRG	Proposed MRG-FF
'70-30'	0.928571429	1
'80-20'	0.6153846	0.923076923
'90-10'	0.901666667	1

To sum up, a tissue with superior quality and higher sensitivity may be more accurately identified using the suggested technique as shown in Fig. 6 (Table 6). When compared to the current MRG approach, our suggested MRG-FF algorithm yields superior results.

6. Conclusion

A picture linked with the Modified Region Growing fruit-fly algorithm was used to classify brain tissue using MRI images. A fuzzy min-max neural network can help in tissue categorization. The MTLAB platform was used with different real-world and medical pictures to execute the suggested study. Following the cleaning of the picture collection, appropriate photos were selected for use in model training and testing. A 70:30, 80:20, and 90:10 ratio was employed for the system. As a result, the final product has improved in terms of quality. It was determined that the planned study satisfied the criteria for sensitivity, specificity, and accuracy. There was also a comparison done between the current MRG and the new MRG-ff. The comparative findings show that the suggested work surpasses the previous work in tissue categorization, delivering superior outcomes. The suggested study has a 95% accuracy rate, which is higher than previous work in the same field. As a result, it outperforms the competition. Because of this, future work in medical image processing and analysis will be motivated by the ideas presented in this proposal.

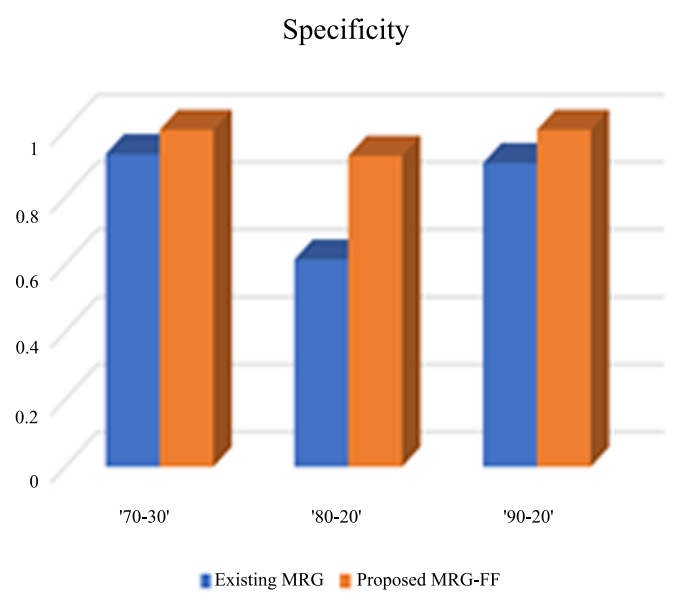

Fig. 6. Graph for proposed and existing specificity value taken based on training and testing values.

Declaration of competing interest

Author declares that there is no conflict of interest.

References

[1] Zaineb B. Messaoud, Siwar Chnitti, Ines Njeh, An automated MRI brain tissue segmentation approach, in: Proc. of the 2nd International Conference on Advanced Technologies for Signal and Image Processing, Monastir, Tunisia, March 2016, pp. 370–374.
[2] G.A. Jothi, H.B. Hannah Inbarani, Hybrid tolerance rough set–firefly based supervised feature selection for MRI brain tumor image classification, Appl. Soft Comput. 46 (September 2016) 639–651.
[3] Toufique Ahmed Soomro, Junbin Gao, Neural network based denoised methods for retinal fundus images and MRI brain images, in: Proc. of the International Joint Conference on Neural Networks (IJCNN), Canada, July 2016, pp. 1151–1157.
[4] Ruey-Maw Chen, Chuin-Mu Wang, MRI brain tissue classification using unsupervised optimized extenics-based methods, in: Porc. of the International Symposium on Computer, Consumer and Control, China, July 2016, pp. 502–505.
[5] Hadeel N. Abdullah, Mustafa A. Habtr, Brain tumor extraction approach in MRI images based on soft computing techniques, in: Proc. of the 8th International Conference on Intelligent Networks and Intelligent Systems, 2015.
[6] Xiaoyun Liu, Fen Chen, Automatic segmentation of 3-D brain MR images by using global tissue spatial structure information, Proc. IEEE Trans. Appl. Supercond. 24 (5) (October 2014).
[7] T. Kalaiselvi, K. Somasundaram, Fuzzy C-means technique with histogram based centroid initialization for brain tissue segmentation in MRI of head scans, in: Proc. of the International Symposium on Humanities, Science and Engineering Research, Location, 2011.

[8] K.S. Thara, K. Jasmine, Brain tumour detection in MRI images using PNN and GRNN, in: Proc. of the Presented at the IEEE WiSPNET Conference, Chennai, March 2016, pp. 1504–1510.
[9] Noramalina Abdullah, Lee Wee Chuen, Umi Kalthum Ngah, Khairul Azman Ahmad, Improvement of MRI brain classification using principal component analysis, in: Proc. of the IEEE International Conference on Control System, Computing and Engineering, 2011, pp. 557–561.
[10] Zarita Zainuddina, Ong Paulinea, An effective fuzzy C-means algorithm based on symmetry similarity approach, in: Proc. of the Applied Soft Computing, vol. 35, October 2015, pp. 433–448.
[11] Fa Zhu, Jian Yang, Junbin Gao, Chunyan Xu, Extended nearest neighbor chain induced instance-weights for SVMs, Pattern Recognit. 60 (December 2016) 863–874.
[12] Piero Baraldia, Francesco Cannarile, Francesco Di Maioa, Enrico Zio, Hierarchical k-nearest neighbours classification and binary differential evolution for fault diagnostics of automotive bearings operating under variable conditions, Eng. Appl. Artif. Intell. 56 (November 2016) 1–13.
[13] Zhaobin Cui, Ying Wang, Xinbo Gao, Jie Li, Yu Zheng, Multispectral image classification based on improved weighted MRF Bayesian, Neurocomputing 212 (November 2016) 75–87.
[14] Alireza Ghaemia, Esmat Rashedia, Ali Mohammad Pourrahimib, Mehdi Kamandara, Farhad Rahdaric, Automatic channel selection in EEG signals for classification of left or right hand movement in brain computer interfaces using improved binary gravitation search algorithm, Biomed. Signal Process. Control 33 (March 2017) 109–118.
[15] Zafer Iscan, Zümray Dokur, Tamer Ölmez, Tumor detection by using Zernike moments on segmented magnetic resonance brain images, Expert Syst. Appl. 37 (3) (2010) 2540–2549.
[16] Anthony Bianchi, Bir Bhanu, Virginia Donovan, Andre Obenaus, Visual and contextual modeling for the detection of repeated mild traumatic brain injury, IEEE Trans. Med. Imaging 33 (1) (2014).
[17] Dongjin Kwon, Marc Niethammer, Hamed Akbari, Michel Bilello, Christos Davatzikos, Kilian M. Pohl, PORTR: pre-operative and post-recurrence brain tumor registration, IEEE Trans. Med. Imaging 33 (3) (2014).
[18] Ashraf Anwar, Arsalan Iqbal, Image processing technique for brain abnormality detection, Int. J. Image Proc. (IJIP) 7 (1) (2013).
[19] Atiq Islam, Syed M.S. Reza, Khan M. Iftekharuddin, Multi-fractal texture estimation for detection and segmentation of brain tumors, IEEE Trans. Biomed. Eng. 60 (11) (2013).
[20] Evangelia I. Zacharaki, Anastasios Bezerianos, Abnormality segmentation in brain images via distributed estimation, IEEE Trans. Inf. Technol. Biomed. 16 (3) (2012).
[21] Christakis Damianou, Kleanthis Ioannides, Venos Hadjisavvas, Nicos Mylonas, Andreas Couppis, Demitris Iosif, In vitro and in vivo brain ablation created by high-intensity focused ultrasound and monitored by MRI, IEEE Trans. Ultrason. Ferroelectr. Freq. Control 56 (6) (2009).
[22] Selva Bhuvaneswari, P. Geetha, Devi Kowsalya, Semantic classification and region growing of brain MRI using CANFIS model for tumor identification, J. Basic Appl. Sci. 8 (3) (March 2014) 43–52.
[23] Daniel Schwarz, Tomas Kasparek, Ivo Provaznik, Jiri Jarkovsky, A deformable registration method for automated morphometry of MRI brain images in neuropsychiatric research, IEEE Trans. Med. Imaging 26 (4) (2007).
[24] K. Gulati, Raja Sarath Kumar Boddu, D. Kapila, S.L. Bangare, et al., A review paper on wireless sensor network techniques in Internet of things (IoT), Mater. Today Proc. (2021), https://doi.org/10.1016/j.matpr.2021.05.067.
[25] S.L. Bangare, G. Pradeepini, S.T. Patil, Implementing tumor detection and area calculation in MRI image of human brain using image processing techniques, Int. J. Eng. Res. Appl. (Part 6) (ISSN 2248-9622) 5 (4) (April 2015) 60–65.
[26] S.L. Bangare, S.T. Patil, et al., Reviewing Otsu's method for image thresholding, Int. J. Appl. Eng. Res. 10 (9) (2015) 21777–21783.
[27] S.L. Bangare, G. Pradeepini, S.T. Patil, Regenerative pixel mode and tumor locus algorithm development for brain tumor analysis: a new computational technique for precise medical imaging, Int. J. Biomed. Eng. Tech. 27 (1/2) (2018).
[28] S.L. Bangare, G. Pradeepini, S.T. Patil, Neuroendoscopy adapter module development for better brain tumor image visualization, Int. J. Elect. Comput. Eng. (IJECE) 7 (6) (December 2017) 3643–3654.
[29] Rajesaheb R. Kadam, Manoj L. Bangare, A survey on security issues and solutions in live virtual machine migration, Int. J. Adv. Found. Res. Comput. (IJAFRC) (ISSN 2348-4853) (December 2012).
[30] Sachindra K. Chavan, Manoj L. Bangare, Secure CRM cloud service using RC5 algorithm, Int. J. Comput. Trends Tech. 4 (3) (2013) 325–330.
[31] Manoj L. Bangare, Sarang A. Joshi, Kernel interpolation-based technique for privacy protection of pluggable data in cloud computing, Int. J. Cloud Comput. 9 (2–3) (2020) 355–374.
[32] S.L. Bangare, S. Gupta, M. Dalal, A. Inamdar, Using node. Js to build high speed and scalable backend database server, in: Proc. NCPCI. Conf. 2016, 2016, p. 19.
[33] Kamal Gulati, V.P. Sriram, Dr. Mukta Sharma Parul, Sherin Eliyas, Sunil L. Bangare, Use for graphical user tools in data analytics and machine learning application, Turkish J. Physiother. Rehabil. (ISSN 2651-4451) 32 (3) (2021).
[34] L.M.I. Leo Joseph, S.L. Bangare, et al., Methods to identify facial detection in deep learning through the use of real-time training datasets management, Eflatounia (ISSN 1110-8703) 5 (2) (2021) 1298–1311.
[35] Shashikant Athawale, Virat Giri, S.L. Bangare, Collateral extension in provocation of security in IoT, Int. J. Future Gener. Commun. Netw. (Web of Science) (ISSN 2233-7857) 14 (1) (2021) 3703–3716.
[36] S.L. Bangare, Brain tumor detection using machine learning approach, Des. Eng. (Scopus Index-Q4) (ISSN 0011-9342) 7 (2021) 7557–7566.
[37] M.L. Bangare, P.M. Bangare, R.S. Apare, S.L. Bangare, Fog computing based security of IoT application, Des. Eng. (Scopus Index-Q4) (ISSN 0011-9342) (7) (2021) 7542–7549.
[38] S.L. Bangare, P.S. Bangare, K.P. Patil, Internet of things with green computing, Turkish J. Physiother. Rehabil. (ISSN 2651-4451) 32 (3) (2021) 12494–12497.
[39] Md Khairul Islam, Md Shahin Ali, Md Sipon Miah, Md Mahbubur Rahman, Md Shahariar Alam, Mohammad Amzad Hossain, Brain tumor detection in MR image using superpixels, principal component analysis and template based K-means clustering algorithm, Mach. Learn. Appl. (ISSN 2666-8270) 5 (2021) 100044, https://doi.org/10.1016/j.mlwa.2021.100044.
[40] G. Ramkumar, R. Thandaiah Prabu, Ngangbam Phalguni Singh, U. Maheswaran, Experimental analysis of brain tumor detection system using machine learning approach, Mater. Today Proc. (ISSN 2214-7853) (2021), https://doi.org/10.1016/j.matpr.2021.01.246.
[41] Linjuan Ma, Fuquan Zhang, End-to-end predictive intelligence diagnosis in brain tumor using lightweight neural network, Appl. Soft Comput. (ISSN 1568-4946) 111 (2021) 107666, https://doi.org/10.1016/j.asoc.2021.107666.